Bull Math Biol
DOI 10.1007/s11538-010-9594-4

ORIGINAL ARTICLE

Instabilities on Prey Dynamics in Jellyfish Feeding

Themistoklis Sapsis · Jifeng Peng · George Haller

Received: 8 November 2009 / Accepted: 11 October 2010

Abstract We study the dynamics of plankton in the wake of a jellyfish. Using an analytical approach, we derive a reduced-order equation that governs the prey motion which is modeled as neutrally-buoyant inertial particle. This modified equation takes into account both the effects of prey inertia and self-propulsion and enables us to calculate both the attracting and repelling Lagrangian coherent structures for the prey motion. For the case of zero self-propulsion, it is simplified to the equation of motion for infinitesimal fluid particles. Additionally, we determine the critical size of prey over which instabilities on its motion occur resulting in different dynamics from those predicted by the reduced-order equation even for the case of zero self-propulsion. We illustrate our theoretical findings through an experimentally measured velocity field of a jellyfish. Using the inertial equation, we calculate the Lagrangian coherent structures that characterize prey motion as well as the instability regions over which larger prey will have different dynamics even for the case of zero self-propulsion.

Keywords Prey inertia and self-propulsion · Prey-size instabilities · Inertial particles · Inertial Lagrangian coherent structures · Reduced order dynamics

T. Sapsis (✉)
Department of Mechanical Engineering, Massachusetts Institute of Technology, Cambridge, MA 02139, USA
e-mail: sapsis@mit.edu

J. Peng
Department of Mechanical Engineering, University of Alaska Fairbanks, Fairbanks, AL 99775-5905, USA
e-mail: jpeng@alaska.edu

G. Haller
Department of Mechanical Engineering, McGill University, Montreal, QC H3A 2K6, Canada
e-mail: george.haller@mcgill.ca

Published online: 26 October 2010

1 Introduction

Medusae are important predators in coastal ecosystems. They feed on zooplankton, fish eggs, and larvae and, therefore, directly influence plankton ecosystems and natural fishery resources (Purcell and Grover 1990; Matsakis and Conover 1991). Medusae are also known to indirectly influence structures of marine planktonic ecosystems through cascades and interactions among different trophic levels in the marine food web (Purcell and Decker 2003). With more frequent and substantial medusan population outbreaks in recent years (Kawahara et al. 2006; Purcell et al. 2007), it is important to understand medusan predatory activities and how they affect marine ecosystems.

One of the most important processes in medusae predation is prey encounter and capture. Laboratory and field studies have identified several important parameters in this process, such as bell diameter (Bailey and Batty 1983), nematocyst type (Purcell and Mills 1991), tentacle orientation and placement (Madin 1988), etc. Other morphological and physiological factors like bell shape and muscle strength can also indirectly affect prey capture capability through swimming speed (Madin 1988) and feeding modes (Colin et al. 2003).

Estimation of trophic effects of medusae also requires better understanding of the variability of prey selection across different medusan species. Medusan dietary preferences for prey organisms have been demonstrated in many studies using selected prey (Hansson et al. 2005) and gut content analyses (Costello et al. 2008; Purcell 2005). These studies suggest that the preferences are results of physical processes during capture and ingestion, and that they depend on multiple parameters including prey size, escape capability, and digestibility. However, the relative importance of these parameters for different medusae species is still unclear. Due to the lack of a more general understanding of the prey selection process, results in empirical studies are usually limited to a small number of readily observable species and cannot be used to predict predation by other species.

A deeper understanding of prey capture and selection mechanisms requires the development of physical model describing the animal-fluid interactions that underlie the capture and selection processes. Such a model can potentially test different hypotheses regarding prey capture and selection. It can also enable independent control of governing parameters in a manner that is more difficult to achieve in field and laboratory studies. Recent studies on large cruising scyphomedusae have made progress in this regard. Contrary to small hydromedusae that primarily wait in ambush (Madin 1988), these large scyphomedusae swim continuously and forage simultaneously. The concurrent activities of swimming and prey-capturing suggest that fluid motion generated during swimming also strongly affect feeding capabilities of scyphomedusae (Colin et al. 2003). Using analytical tools from fluid dynamics and dynamical systems, Shadden et al. (2006) developed a mechanistic model that quantified fluid motions during swimming of scyphomedusae *Aurelia aurita* and identified a region in which the fluid can interact with the capture surface. Peng and Dabiri (2009) further developed the model to incorporate effects of prey properties and behaviors on capture and selection. The model considers prey as small particles whose motions are determined by the surrounding flow and several prey parameters, such as prey size,

capabilities of perceiving predators, and generating escape swimming force. The effect of these parameters on prey capture and selection are quantified by measuring the size of capture region, i.e., the region in which prey can interact with the capture surface.

Though the model was able to demonstrate prey selection based on prey size, capabilities of perceiving predators, and generating escape swimming force, it did so by measuring the size of capture region, a collective of prey capture. It did not consider individual prey dynamics nor answer the question why some prey are captured and why others are not. The computation of the capture region was based on the calculation of the Lagrangian coherent structures for small spherical inertial particles, modeling the prey. For fluid flows, Lagrangian coherent structures (or LCS) can be defined as smooth sets of fluid particles with distinguished stability properties. Specifically, repelling (or forward) LCS are material surfaces that repel all neighboring fluid trajectories; similarly, attracting (or backward) LCS attract all neighboring fluid trajectories. These definitions are objective, i.e., invariant with respect to translations and even time-varying rotations of the coordinate frame. Therefore, LCS can be used to explain the forward and backward-time behavior of typical infinitesimal fluid particles. To extract Lagrangian structures from the flow, one may use the direct or finite-time Lyapunov-exponent (FTLE) method developed in Haller (2001). For the inertial particles dynamics, this computation requires the numerical solution of the Maxey–Riley equation (a four-dimensional singular perturbation problem), which is a very expensive process for the calculation of repelling LCS and an impossible computation for the attracting LCS due to the numerical ill-posedness of the advection problem backward in time.

In this work, we use recent tools from dynamical systems theory to describe the motion of prey through a reduced-order equation without singular terms. More specifically, in Haller and Sapsis (2008), a general reduced-order equation (*inertial equation*) for the asymptotic motion of spherical finite-size particles in unsteady fluid flows was derived. The corresponding reduced inertial velocity field is a small perturbation of the ambient velocity field, with the order of the perturbation defined as the size of the inertial particle relative to characteristic length scale in the flow. Due to this perturbation in velocity, inertial particle motion can develop substantial differences from infinitesimal particle motion in the same ambient flow field. For the analysis of prey motion, we use *inertial Lagrangian coherent structures* (ILCS), defined in Sapsis and Haller (2009a), as LCS extracted from the inertial equation by the finite-time Lyapunov-exponent method. Specifically, *attracting ILCS* attract finite-size particles, while *repelling ILCS* repel finite-size particles. The network of repelling and attracting ILCS form the inertial analogue of tangled networks known from simple examples of chaotic advection of infinitesimal fluid particles.

It turns out, however, that for larger particle sizes, instabilities in the dynamics of inertial particles will develop (Sapsis and Haller 2009b). These instabilities drive away inertial particle trajectories from the slow manifold on which the inertial equation is valid. As a result, in a given flow, an attracting ILCS may only stay attracting for smaller particles, while larger particles ultimately spin away from the ILCS due to their inertia. Such "spin-offs" happen in regions of high strain; the exact strain threshold is derived in Sapsis and Haller (2009b) for neutrally buoyant particles without self-propulsion.

In this work, we use and formulate the above dynamical system tools in the context of prey-motion to study the effect of the prey inertia as well as its self-propulsion. Using the derived reduced-order inertial equation, we are able to calculate rigorously ILCS and compute analytically the regions where instabilities on the prey motion, due the combined effect from its size and self-propulsion, will occur. In contrast to previous studies on the subject where coherent structures were computed purely by analogy with infinitesimal LCS, the current study computes ILCS on a slow manifold that is globally attracting. The reduced order of the inertial equation allows also for the calculation of attracting ILCS, a computation which was not feasible by trying to solve backward the full Maxey–Riley equation (since Maxey–Riley is numerically unstable in backward time due to the singular term; see Haller and Sapsis 2008). For larger values of prey inertia, we study the dynamical mechanism that allows prey to escape from the capture region. This is due to a normal instability of the slow manifold that occurs in specific subsets of the physical domain described by an analytical condition. We illustrate the role of these regions by numerically solving the full equation of motion and show that larger prey may escape from the capture region which has been computed using the repelling ILCS. This is because in these regions the dynamical instabilities cause divergence of the prey velocity from the one imposed by the slow manifold and thus the inertial equation is not valid. We also prove that the existence of prey self-propulsion (with specific characteristics) always causes reduction of there regions. Therefore, the computed ILCS are the relevant structures for prey motion if the prey size is smaller than a critical value which can be determined explicitly using the presented techniques.

2 Prey Dynamics

Let $\mathbf{x}$ refer to three-dimensional spatial locations and let t denote time. Let $\mathbf{u}(\mathbf{x}, t)$ denote the three-dimensional velocity field of the flow of density ρ_f due to the motion of the jellyfish. For simplicity, we neglect the body shape of the prey and consider it as small spherical particles of density ρ_p and radius a. Hence, the prey dynamics can be described by the Maxey–Riley equation. However, the forces on the right-hand side of the Maxey–Riley equation only include fluid forces acting on passive particles due to the background fluid currents and gravity. Small plankton are capable of self-propulsion, often triggered by perception of a nearby predator. This effect was modeled in Peng and Dabiri (2009) by the addition of a term on the rhs of the Maxey–Riley equation representing the acceleration rate $\mathbf{a}_e$ of prey animals due to the self-generated escape force. This escape force may be dependent on time and the local flow characteristics, e.g., local shear stress. Because most microscopic aquatic animals are neutrally buoyant, we assume $\rho_f = \rho_p$. Therefore, the dynamics of a prey animal can be expressed as (Peng and Dabiri 2009)

$$\begin{aligned} \dot{\mathbf{x}} &= \mathbf{v}, \\ \epsilon\dot{\mathbf{v}} &= \mathbf{u}(\mathbf{x},t) - \mathbf{v} + \epsilon\frac{D\mathbf{u}(\mathbf{x},t)}{Dt} + \epsilon\mathbf{a}_e\big(\mathbf{u}(\mathbf{x},t)\big), \end{aligned} \tag{1}$$

where

$$\epsilon = \frac{1}{\mu} \ll 1, \qquad \mu = \frac{2}{3St}, \qquad St = \frac{2}{9}\left(\frac{a}{L}\right)^2 \mathrm{Re},$$

with Re denoting the flow Reynolds number. We also assume explicit dependence of the self-propulsion term only on the local flow field even though the following analysis holds for general explicit dependence on space and time. Without the escape acceleration term $\mathbf{a}_e$, (1) is the linearized Maxey–Riley equation for neutrally buoyant spherical particles (cf., e.g., Maxey and Riley 1983; Benczik et al. 2002 or Babiano et al. 2000). The equation has been nondimensionalized by length scale L (the radius of the jellyfish), characteristic velocity U (the jellyfish swimming speed), and characteristic time $T = L/U$.

Note that (1) is a nonautonomous six-dimensional differential equation for 3D flows and four-dimensional for 2D flows. In addition to its temporal and dimensional complexity, (1) also involves a singular perturbation problem due to the small parameter ϵ on the left-hand side. This causes a strong exponential instability when one attempts to solve the equations in backward time to locate attracting invariant manifolds in the six/four-dimensional phase space (see, e.g., Haller and Sapsis 2008).

2.1 Reduced Order Dynamics

In Haller and Sapsis (2008), it is proven that for $\epsilon > 0$ small enough, (1) without the acceleration term $\mathbf{a}_e$, admits a globally attracting invariant slow manifold. This three-dimensional time-dependent surface of particle trajectories can be calculated explicitly up to any order of precision also for the case of nonzero acceleration $\mathbf{a}_e$. Here, we follow the same methodology presented in Haller and Sapsis (2008) to derive a reduced-order inertial equation that takes into account the prey self-propulsion term. Specifically, Haller and Sapsis (2008) show for $a_e(\mathbf{u}(\mathbf{x},t)) = 0$ the existence of $\epsilon_0 > 0$, such that for all $\epsilon \in [0, \epsilon_0)$, system (1) admits an attracting locally invariant slow manifold M_ϵ that can be written in the form of a Taylor expansion

$$\begin{aligned} M_\epsilon = \big\{(\mathbf{x}, t, \mathbf{v}) :\ \mathbf{v} = \mathbf{u}(\mathbf{x}, t) + \epsilon \mathbf{u}^1(\mathbf{x}, t) + \cdots \\ + \epsilon^r \mathbf{u}^r(\mathbf{x}, t) + \mathcal{O}\big(\epsilon^{r+1}\big),\ (\mathbf{x},\ t) \in D_0\big\}; \end{aligned} \tag{2}$$

the functions $\mathbf{u}^k(\mathbf{x}, t)$ are as smooth as the right-hand side of (1). Inclusion of the acceleration term $\mathbf{a}_e$ in (1) does not modify this result. Therefore, following the same approach, we find the new functions $u^k(x, t)$ using the invariance of M_ϵ, which allows us to differentiate the equation defining M_ϵ in (2) with respect to t. Specifically, differentiating

$$\mathbf{v} = \mathbf{u}(\mathbf{x}, t) + \sum_{k=1}^{r} \epsilon^k \mathbf{u}^k(\mathbf{x}, t) + \mathcal{O}\big(\epsilon^{r+1}\big)$$

with respect to t gives

$$\dot{\mathbf{v}} = \mathbf{u}_\mathbf{x}\dot{\mathbf{x}} + \mathbf{u}_t + \sum_{k=1}^{r} \epsilon^k \big[\mathbf{u}^k_\mathbf{x}\dot{\mathbf{x}} + \mathbf{u}^k_t\big] + \mathcal{O}\big(\epsilon^{r+1}\big), \tag{3}$$

on M_ϵ, where subscripts denote differentiation with respect to the corresponding argument (except of the acceleration $\mathbf{a}_e$). Restricting the $\mathbf{v}$ equations in (1) to M_ϵ gives

$$\begin{aligned}\epsilon\dot{\mathbf{v}} &= \left[\mathbf{u}-\mathbf{v}+\epsilon\frac{D\mathbf{u}}{Dt}+\epsilon\mathbf{a}_e\right]_{M_\epsilon}\\ &= -\sum_{k=1}^{r}\epsilon^k\mathbf{u}^k(\mathbf{x},t)+\epsilon\frac{D\mathbf{u}}{Dt}+\epsilon\mathbf{a}_e.\end{aligned} \tag{4}$$

Comparing terms containing equal powers of ϵ in (3) and (4), then passing back to the original time t, we obtain the following result.

Theorem 1 *For sufficiently small prey mass $\epsilon > 0$ and in presence of the self-propulsion term $\mathbf{a}(\mathbf{u})$, the asymptotic equation of motion for the prey can be written as*

$$\dot{\mathbf{x}} = \mathbf{u}_\epsilon(\mathbf{x},t) \equiv \mathbf{u}(\mathbf{x},t) + \epsilon\mathbf{u}^1(\mathbf{x},t) + \cdots + \epsilon^r\mathbf{u}^r(\mathbf{x},t) + \mathcal{O}\left(\epsilon^{r+1}\right), \tag{5}$$

where r is an arbitrary but finite integer, and the functions $\mathbf{u}^i(\mathbf{x},t)$ are given by

$$\begin{aligned}&\mathbf{u}^1(\mathbf{x},t) = \mathbf{a}(\mathbf{u}),\\ &\mathbf{u}^k(\mathbf{x},t) = -\left\{\mathbf{u}_t^{k-1} + \sum_{i=0}^{k-1}\mathbf{u}^i\nabla\mathbf{u}^{k-i-1}\right\}, \quad k \geq 2.\end{aligned} \tag{6}$$

with $\mathbf{u}^0(\mathbf{x},t) \equiv \mathbf{u}(\mathbf{x},t)$.

We shall refer to (5) with the $\mathbf{u}^i(\mathbf{x},t)$ defined in (6) as the *inertial equation* associated with the velocity field $\mathbf{u}(\mathbf{x},t)$, because (5) gives the general asymptotic form of inertial particle motion induced by $\mathbf{u}(\mathbf{x},t)$. A leading-order approximation to the inertial equations is given by

$$\dot{\mathbf{x}} = \mathbf{u}(\mathbf{x},t) + \epsilon\mathbf{a}_e. \tag{7}$$

The above argument renders the slow manifold M_ϵ over the fixed time interval $[t_0 - T, t_0 + T]$. Since the choice of t_0 and T was arbitrary, we can extend the existence result of M_ϵ to an arbitrary long finite time interval.

2.2 Instability Regions

For the case where prey has no self-propulsion, the slow manifold is simplified to the fluid velocity field $\mathbf{u}(\mathbf{x},t)$. Therefore, particles should synchronize exponentially fast with fluid elements motion. By contrast, Babiano et al. (2000) and Vilela et al. (2006) give numerical evidence that two-dimensional suspensions do not approach fluid elements motions; instead, their trajectories scatter around unstable manifolds of the Lagrangian dynamics. The above phenomenon has been studied in Sapsis and Haller (2009b) where it is shown that for larger values of ϵ, the slow manifold M_ϵ

looses its stability in certain regions of the configuration space. These instability regions where divergence from the slow manifold will occur are described explicitly by an analytical expression for any given velocity field. In Haller and Sapsis (2009), this analysis is extended for the case of general dynamical systems that contain an invariant manifold.

These dynamical instabilities play an important role on the motion of plankton close to the jellyfish since they allow larger-sized prey to escape from its predator even though the former lies inside the capturing region defined by the repelling LCS. This can happen because over unstable regions of the slow manifold, we have divergence of prey velocity from the one given by the reduced-order dynamics, and thus the inertial equation (5), used to compute LCS, is not valid. To identify such unstable domains, as well as the critical size of prey over which these domains exist, we apply the theorem proven in Haller and Sapsis (2009) and we obtain the following result for the case of self-propulsion.

Theorem 2 *For prey having mass* $\epsilon > 0$, *its velocity* $\mathbf{v}(t)$ *converges to* $\mathbf{u}_\epsilon(\mathbf{x},t)$ *if and only if*

$$s(\mathbf{x},t) \equiv \lambda_{\max}\left[-\frac{\nabla\mathbf{u}_\epsilon(\mathbf{x},\mathbf{t})+[\nabla\mathbf{u}_\epsilon(\mathbf{x},t)]^T}{2}\right]-\frac{1}{\epsilon}<0; \tag{8}$$

where $\lambda_{\max}[A]$ *denotes the maximal eigenvalue of a tensor* A; A^T *is the transpose of* A.

3 Prey Transport

In this section, we study the motion of prey in the realistic velocity field of a jellyfish which has been measured experimentally. Using the inertial equation (5) derived previously, we calculate the attracting and repelling ILCS. Subsequently, we calculate the unstable domains of the slow manifold for a specific size of prey and study their role on prey motion by solving the full four-dimensional Maxey–Riley equation.

3.1 Flow Generation and Measurement

Juvenile jellyfish *Aurelia aurita* were collected from Cabrillo Marine Aquarium (San Pedro, CA) and kept in a 75-gallon acrylic pseudokreisel tank with seawater at 14°C. The velocity fields generated by free-swimming jellyfish were measured by digital particle image velocimetry (DPIV) (Fig. 1). A pulsed laser of 30 Hz was focused into a thin light sheet 1 mm thick and illuminated a two-dimensional plane in the flow. Reflective silver-coated neutrally-buoyant hollow glass spheres (mean diameter 13 μm) were added into the tank and their motion were video-taped using a Uniq camera with 1024 × 1024 resolution at frame rate of 30 Hz synchronized with the laser. The camera image plane was parallel to the laser plane. Video sequences of jellyfish swimming with their body symmetry on the laser plane for several consecutive swimming cycles were collected for analysis. These sequences were analyzed using an in-house DPIV analysis system to quantify velocity field

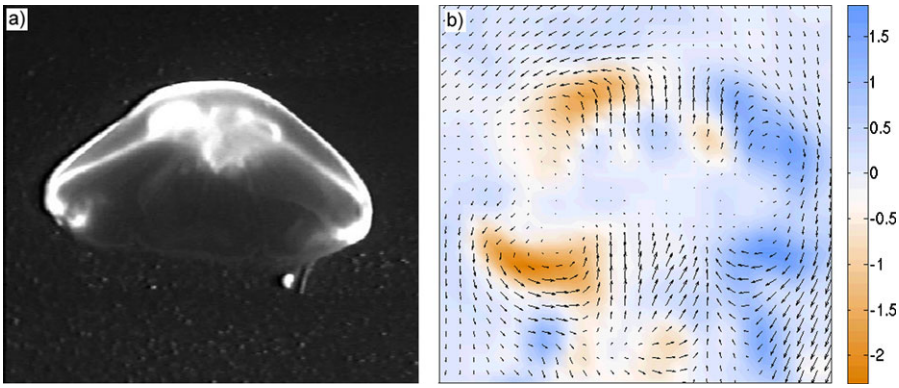

Fig. 1 (Color online) (**a**) Juvenile jellyfish *Aurelia aurita*. (**b**) Measured velocity field. The *color* on the plot represents the vorticity field

measurements of the flow. For additional details of the experiments, please refer to previous studies on swimming properties of the same species (Shadden et al. 2006; Franco et al. 2007).

The characteristic length scale of the flow was set by the radius of the jellyfish, $L = 5$ cm and the characteristic velocity by the jellyfish swimming speed, $U = 1$ cm/s. The corresponding Reynolds number of the flow was given by $\mathrm{Re} = 500$. To model the self-propulsion of the prey, we assume a hypothetical prey escape mechanism in which the escape force has the form

$$\mathbf{a}_e = -a_e \frac{\mathbf{u}}{|\mathbf{u}|}$$

that represents a force with its direction always opposite to the local flow velocity (see Peng and Dabiri 2009). It is also assumed that the escape force is persistent, and thus the acceleration has a smaller value, with the magnitude $a_e = 25$ in nondimensionalized units.

3.2 Inertial Lagrangian Coherent Structures

For fluid flows, LCS are distinguished sets of fluid trajectories that govern the forward-time and backward-time asymptotics of other fluid particles. They can be located by calculating Direct Lyapunov Exponents (or FTLE, see below) from the Lagrangian equation of motion $\dot{\mathbf{x}} = \mathbf{u}(\mathbf{x}, t)$ for infinitesimal particles (see Haller 2001). The FTLE method has several advantages over Eulerian methods, including frame independence, greater detail and the ability to define structure boundaries without relying on a preselected threshold. On the downside, as all Lagrangian methods, FTLE relies on the generation of particle paths, and hence is more computationally intensive than Eulerian methods.

In this application, we are interested to locate LCS that impact the motion of *finite-size* particles. Such *inertial LCS* (ILCS) are obtained by applying the FTLE method to the inertial equation (5) and have been studied previously in the context of heavy

particles transport in hurricanes in Sapsis and Haller (2009a). Note that ILCS differ from LCS, since the latter structures are calculated for the infinitesimal particle dynamics governed by $\dot{\mathbf{x}} = \mathbf{u}(\mathbf{x}, t)$.

By solving numerically the inertial equation (5) for a grid of initial conditions $\mathbf{x}_0$ at t_0, we determine the asymptotic inertial particle trajectories $\mathbf{x}(t, \mathbf{x}_0)$. For the numerical solution of the inertial equation, a fourth-order Runge–Kutta algorithm is combined with a cubic interpolation scheme for both space and time to improve accuracy. As initial time, we choose $t_0 = 6$; the integration time interval is chosen for both backward and forward integration $\Delta T = 5$. By numerical differentiation, we compute the largest singular-value field $\lambda_{\max}(t, t_0, \mathbf{x}_0)$ of the deformation-gradient tensor field $\partial \mathbf{x}(t, t_0, \mathbf{x}_0)/\partial \mathbf{x}_0$. Then the ILCS can be represented as the local maximizing sets of the finite-time Lyapunov exponent (FTLE) field $\sigma_{t_0}^{t}(\mathbf{x}_0) = [\ln \lambda_{\max}(t, t_0, \mathbf{x}_0)]/(2(t - t_0))$, over initial positions $\mathbf{x}_0$. To avoid artificial structures due to the finite domain over which the velocity field is measured (see Tang et al. 2010) we neglect a narrow zone of points close to the boundary (3% of the domain size from each side); this does not cause significant loss of information since the important dynamics take place in the interior of the computational domain and not on the boundary.

In Fig. 2, we present the forward and backward FTLE fields for the case of prey without self-propulsion ($a_e = 0$) (a) and for the case where self-propulsion is taken into account ($a_e = 25$) (b). As demonstrated by the backward FLTE field, due to the axisymmetric shape of medusae, the flow is largely axisymmetric, also. However, experimental measurements of the flow in the study has an under-resolved region on one side of the animal because laser light used to illuminate the flow was partially blocked the animal. Thus, the forward FLTE field is not axisymmetric with one side under-resolved than the other. Peng and Dabiri (2009) illustrated that the capture region for prey can be defined as the repelling LCS extracted by the forward FTLE field computed using the full Maxey–Riley equation. Here, we use the reduced-order inertial equation which approximates the prey dynamics successfully for sufficiently small prey sizes. By comparing the two cases, we observe that the presence of self-propulsion reduces the size of the lobes which are in front of the jellyfish (Fig. 2, left column). Similar observations have been made by Peng and Dabiri (2009) using the full Maxey–Riley equation for the computation of LCS.

The use of the inertial equation also enables us to compute the attracting LCS through the computation of the backward FTLE field for the two cases (Fig. 2, right column). Note that the computation of these FTLE fields through the Maxey–Riley equation is not possible due to the numerical ill-posedness of the problem. The lower part of the attracting LCS is strongly correlated with the arms of the jellyfish which are also capturing surfaces and because of their flexibility tend to align with these attracting structures. By comparing the two LCS fields (Fig. 2, right column), we observe that the consideration of particle self-propulsion does not have an important impact on the form of the backward FTLE field.

3.3 Prey Motion Without Self-propulsion

We now consider the case of prey without self-propulsion ($a_e = 0$). First, we compute both the attracting and repelling ILCS (red and green curves, respectively, in Fig. 3)

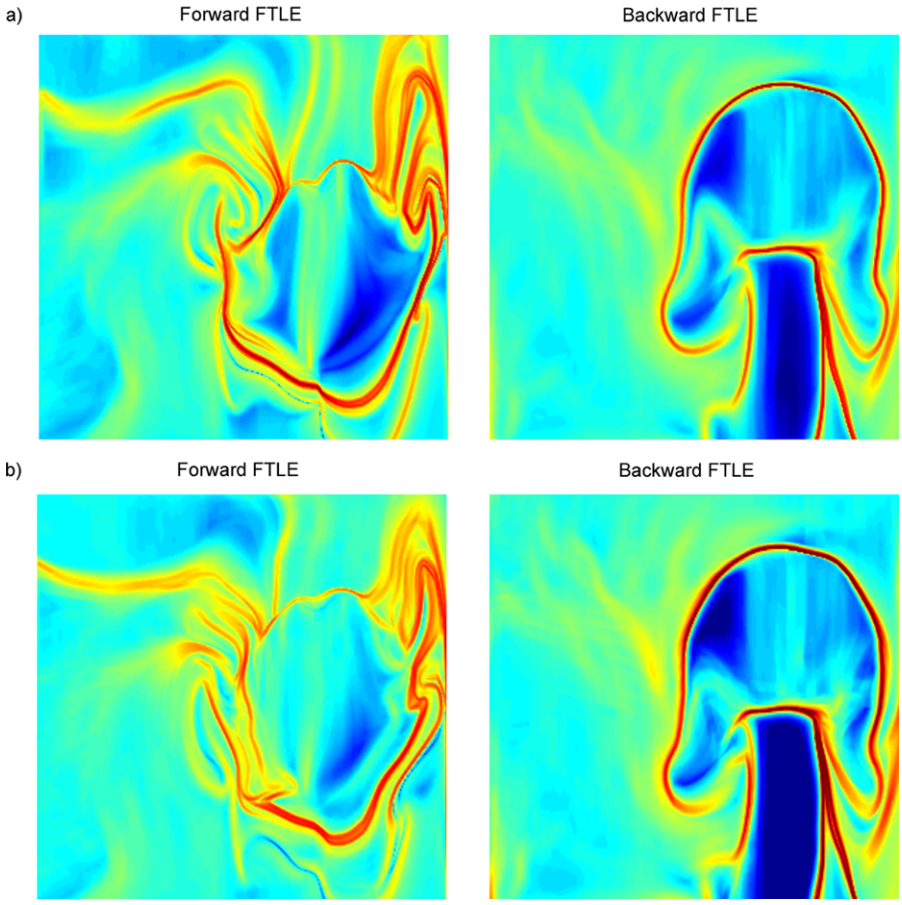

Fig. 2 Forward and backward FTLE fields extracted from the inertial equation (5) for the case of prey with no self-propulsion (**a**) and when self-propulsion is taken into account (**b**)

using the inertial equation for prey size parameter $\epsilon = 0.6$ and for three different time instants $t = 0$, 5.5, and 13.5. Subsequently, we use the analytical criterion (8) to compute the regions of the slow manifold where instabilities will occur (shaded regions). By requiring global stability of the slow manifold, i.e. validity of (8) over the whole domain, we find the maximum prey size $a_{cr} = 1.4$ mm ($\epsilon = 0.09$) for which the reduced-order equation is valid. To illustrate the instability effects, we will consider the case of much larger prey size so that instabilities regions occur in the flow. As it was discussed previously, over those regions the motion of prey is no longer described by the inertial equation (5). We initiate three pairs of particles. Each pair consists of a neutrally buoyant particle with $\epsilon = 0.6$ advected using the inertial equation where the dynamics are reduced on the slow manifold (white dots—yellow trajectories) and one particle advected using the full Maxey–Riley equation (blue dots—black trajectories). The two particles of each pair are initiated in the same locations (Fig. 3, left panel) which lie inside the capturing region predicted according

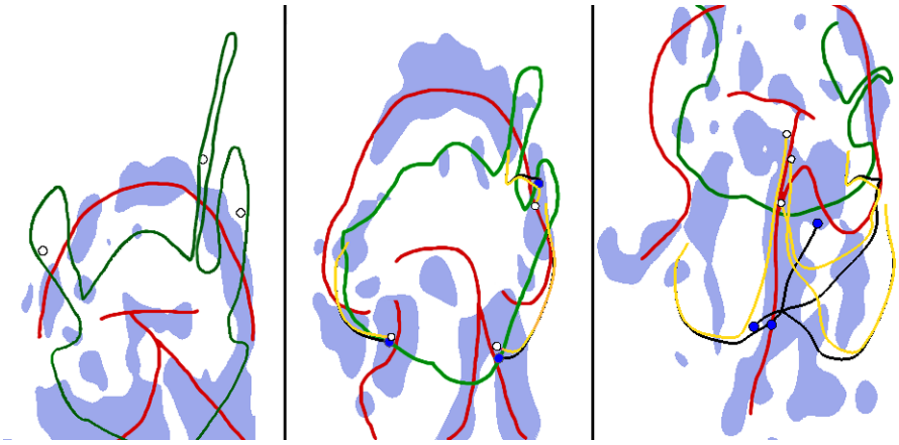

Fig. 3 (Color online) Predator-prey interactions in the absence of self-propulsion for three time instants $t = 0$, 5.5, and 13.5. *White dots*: particles governed by the inertial equation; *blue dots*: particles governed by the full Maxey–Riley equation; *red curve*: attracting ILCS; *green curve*: repelling ILCS; *blue shaded domains*: instability regions

to the repelling (or forward) ILCS. As time evolves, the pairs move together until they enter an instability region (shaded region) where separation begins to occur (Fig. 3, central panel). Over these regions, the dynamics of the blue particles are not governed by the inertial equation and, therefore, ILCS do not act as barriers to their motion. Hence, in the last time instant (Fig. 3, right panel), we can see that even though the white particles, which evolved according to the inertial equation, end up inside the capture region, all the blue particles escaped because of the normal instability of the slow manifold that changed their dynamics. Even though there are initial conditions starting outside the lobes and ending up inside the capture regions those are very few compared with the ones described above.

In Fig. 4, we present two snapshots of inertial particle dynamics viewed in the space of $(x, y, |\mathbf{v}|)$. We show the instantaneous slow manifold M_ϵ as a surface, at two different times; regions encircled by the black solid curves (red regions online) show the domain of local divergence on the slow manifold. The trajectories represent the paths of inertial particles in the $(x, y, |\mathbf{v}|)$ space. The smaller subplots in the figure show the distance $|\mathbf{u} - \mathbf{v}|$ of the particles from the slow manifold (in these plots, therefore, the slow manifold appears as a plane). Note that for the inertial parameter chosen ($\epsilon = 0.6$) the unstable regions are relatively large so that the particles do not end up converging to the slow manifold. They are repelled by the domain of local divergence (regions encircled by the black solid curves) as predicted by our theory.

3.4 Prey Motion in the Presence of Self-propulsion

In this section, we consider the case of prey ($\epsilon = 0.6$) with self-propulsion ($a_e = 25$). The effect of escaping acceleration $\mathbf{a}_e$ on the capture region has been studied in Peng and Dabiri (2009). Specifically, the capture region is determined by directly solving the full Maxey–Riley equation and it shows that the effect of escaping acceleration

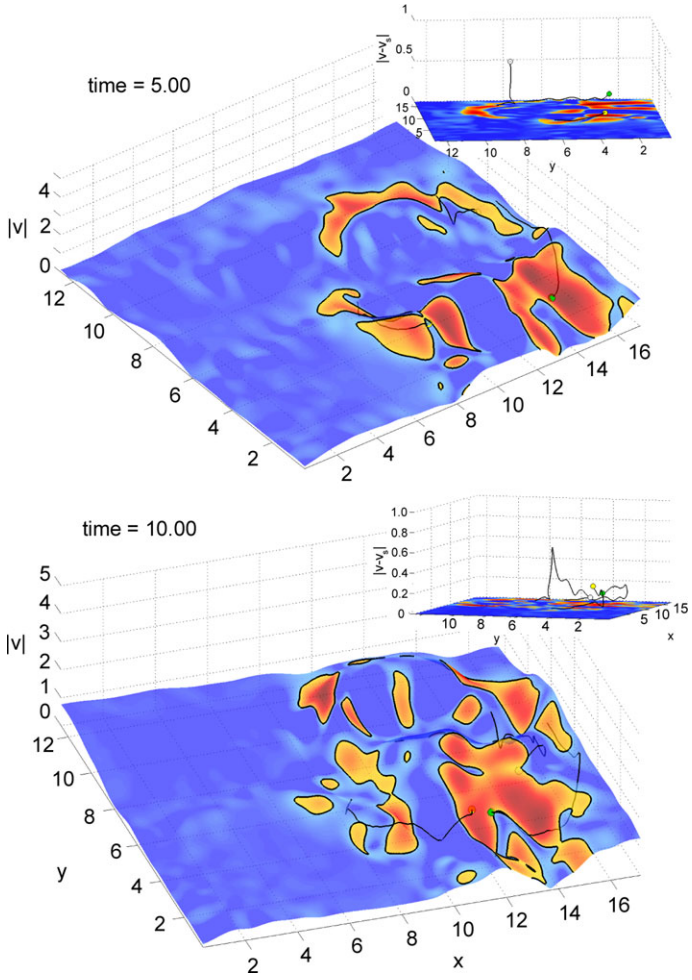

Fig. 4 Convergence of neutrally buoyant particles to the slow manifold M_ϵ, interrupted by regions of divergence along the slow manifold. The repelling domain on the slow manifold, encircled by the *black solid curves*, satisfy formula (8)

$\mathbf{a}_e$ is to decrease the capture region. By assuming that prey capture rate is proportional to the size of capture region, escaping mechanism reduces prey capture rate. Here, we study the dynamical mechanism that results in this observed behavior. Similarly, with the previous section, we first solve the inertial equation (5) (keeping terms up to the third order) to obtain the attracting and repelling ILCS. Those are shown in Fig. 5 for three different time instants: $t = 2$, 6.5, and 14.5 with red and green curves, respectively. The instability regions are also presented as blue shaded domains. Comparing with the previous case, we observe that these regions are reduced in size for the case of prey with self-propulsion although they are still important enough to alter the prey dynamics. To understand this behavior, i.e., smaller instability regions in the presence of self-propulsion, we expand the maximum eigenvalue in the stability

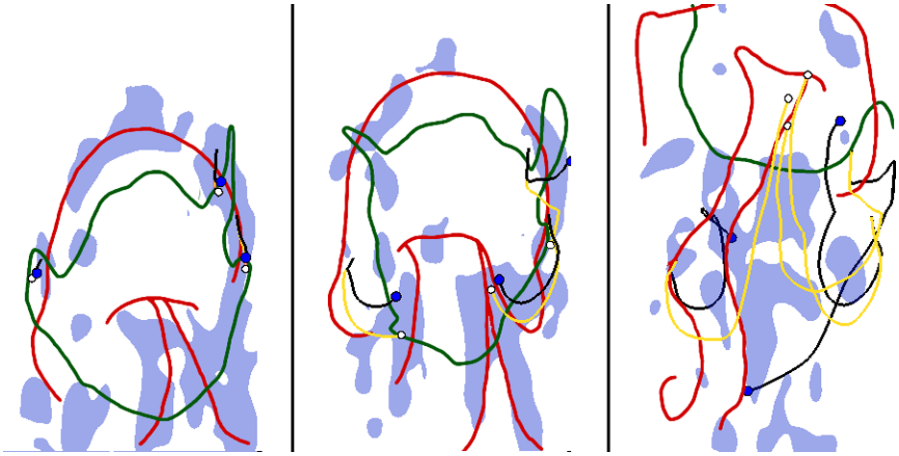

Fig. 5 (Color online) Predator-prey interactions in the presence of self-propulsion for three time instants $t = 2$, 6.5, and 14.5. *White dots*: particles governed by the inertial equation; *blue dots*: particles governed by the full Maxey–Riley equation; *red curve*: attracting ILCS; *green curve*: repelling ILCS; *blue shaded domains*: instability regions

condition (8) taking into account the form of the self-propulsion (in what follows $\mathbf{S_u} \equiv \frac{\nabla \mathbf{u}(\mathbf{x},\mathbf{t}) + [\nabla \mathbf{u}(\mathbf{x},t)]^T}{2}$)

$$\lambda_{\max}\left[-\mathbf{S}_{\mathbf{u}_\epsilon}(\mathbf{x},t)\right] - \frac{1}{\epsilon} < 0 \quad \Leftrightarrow$$

$$\lambda_{\max}\left[-\mathbf{S}_{\mathbf{u}}(\mathbf{x},t) + \epsilon a_e \mathbf{S}_{\frac{\mathbf{u}}{|\mathbf{u}|}}(\mathbf{x},t)\right] - \frac{1}{\epsilon} < 0 \quad \Rightarrow$$

$$\lambda_{\max}[-\mathbf{S}_{\mathbf{u}}(\mathbf{x},t)t] - \epsilon a_e \lambda_{\max}\left[-\mathbf{S}_{\frac{\mathbf{u}}{|\mathbf{u}|}}(\mathbf{x},t)\right] - \frac{1}{\epsilon} + \mathcal{O}(\epsilon^2) < 0.$$

Therefore, the contribution of the self-propulsion term on the existence of unstable regions is always opposite to the inertial effect (which is expressed through the first term). Moreover, since, the fields $\mathbf{u}$ and $\frac{\mathbf{u}}{|\mathbf{u}|}$ have the same geometry (but different magnitude), their strain tensor fields will have eigenvalues with the same sign. Hence, the first order correction due to self-propulsion will always cause smaller instability regions for this type of prey self-propulsion. Additionally, using the above formula, we are able to quantify the effect of prey inertia and self-propulsion on the existence of instability regions by determining the critical values ϵ and a_e over which instabilities will occur for any given self-propulsion pattern.

To illustrate the effect of self-propulsion and inertia on the dynamics of prey, we initiate three pairs of particles inside the capture region computed through the repelling ILCS (green curve). Each one consists of two particles modeling prey with self propulsion, with the first one restricted to move on the slow manifold (white) and the second one evolving according to Maxey–Riley equation including the acceleration term $\mathbf{a}_e$. As we observe, the pairs are initiated into unstable regions, and hence the separation occurs very rapidly as opposed to the previous case where separation

was more delayed since the particles were initiated into a stable part of the slow manifold. As time evolves, two of the blue particles cross the repelling ILCS (i.e., the capture region) and escape. On the other hand, the white particles remain inside the capture region and align with the red curves that define the attracting ILCS. The third particle has also deviated from its pair although the change on its dynamics is not sufficient to pull it out from the capture region.

Note that the effect of prey self-propulsion on their escape depends on the detailed escape behavior. For example, larger prey such as calanoid copepods, are able to generate fast swimming escape upon perception of a predator. During escape responses, they use power stroke to generate maximal swimming force of 40 to 100 dynes, equivalent to an acceleration rate exceeding 100 $\mathrm{m\,s^{-2}}$, over a short span of several hundred ms in average (Lenz and Hartline 1999; Waggett and Buskey 2007). The net effect is a fast jump of 10 mm on average. This fast escape mechanism is more efficient for prey to escape, compared with a slower "cruising" type of escape exhibited by smaller prey such as brine shrimp larvae. Specifically, there are empirical studies (Sullivan et al. 1994; Hansson et al. 2005) showing that rowing medusae like Aurelia Aurita feed mostly on slow escape prey (Artemia salina nauplii and cirripede larvae) with high clearance rate, compared with low clearance rate on fast escape prey (copepods). This prey selection suggested that fast escape mechanism is more efficient. This also explains why jellyfish Aurelia Aurita is a good predator on brine shrimp larvae, and not on copepods.

4 Conclusions

We have studied prey motion in the flow field around a jellyfish. Using an analytic approach, we illustrated that for sufficiently small sizes the prey motion can be captured by a reduced-order inertial equation through the restriction of the dynamics to an invariant slow manifold that governs the motion of finite-size particles. Although the full Maxey–Riley equation for particles motion can only be used for the analysis of repelling ILCS, with the inertial equation we extract both attracting and repelling ILCS that define important collectives for the jellyfish such as the capture region or the locations where the arms of the jellyfish (which are also capturing surfaces) will move. We also illustrated that for larger prey size the slow manifold loses locally its stability and in this case the ILCS are not the relevant structures for the description of prey motion. Using analytical arguments, we have described explicitly the regions where these instabilities will occur.

We have applied our theoretical findings to an experimentally measured velocity field of the jellyfish *Aurelia Aurita*. Using the reduced-order inertial equation, we computed both the attracting and repelling ILCS in order to give a complete characterization of prey motion in the cases where self-propulsion is either ignored or is taken into account. Then, by applying the theoretical results for the stability of the slow manifold, we have determined the critical value of prey size over which instabilities will occur. For larger prey size, the same analysis describes explicitly those locations where the reduced-order inertial equation is no longer valid. By solving the full Maxey–Riley equation we have shown how these instability regions alter the

prey dynamics compared to those predicted by the ILCS. The modified dynamics allow prey to finally escape because of its size, although the ILCS analysis predicts that it should get captured.

Many empirical studies have suggested that prey selection by different medusan species is caused by many factors. However, because the species-specific approach in these empirical studies, their conclusions are difficult to be generalized. One of the biological insights from our study is that the model demonstrates, from a physical and mathematical perspective that prey selection is dependent on a combination of many factors, including characteristics of flow induced by the predator, prey size, self-propulsion, escape strategies, etc. One of the advantages of the model is that compared with empirical studies it is able to isolate the effect of these parameters and potentially determine the dominant factor. This requires further cross-spectrum studies based on the model which, combined with empirical studies, can provide more understanding on prey selection.

Acknowledgements We are grateful to Prof. J. Dabiri for his support during the preparation of this work, and Prof. J. Marsden for suggesting the application of finite-size particles analytical results to the considered problem. We also thank Cabrillo Marine Aquarium in San Pedro, California for providing animals and assistance for the experiments. This research was supported by NSF Grant DMS-04-04845, AFOSR Grant AFOSR FA 9550-06-0092, and a George and Marie Vergottis Fellowship at MIT.

References

Babiano, A., Cartwright, J. H. E., Piro, O., & Provenzale, A. (2000). Dynamics of a small neutrally buoyant sphere in a fluid and targeting in Hamiltonian systems. *Phys. Rev. Lett.*, *84*, 5764.

Bailey, K. M., & Batty, R. S. (1983). A laboratory study of predation by Aurelia aurita on larval herring (Clupea harengus): experimental observations compared with model predictions. *Mar. Biol.*, *72*, 195–301.

Benczik, I. J., Toroczkai, Z., & Tél, T. (2002). Selective sensitivity of open chaotic flows on inertial tracer advection: catching particles with a stick. *Phys. Rev. Lett.*, *89*, 164501.

Colin, S. P., Costello, J. H., & Klos, E. (2003). In situ swimming and feeding behaviour of eight co-occurring hydromedusae. *Mar. Ecol. Prog. Ser.*, *253*, 305–309.

Costello, J. H., Colin, S. P., & Dabiri, J. O. (2008). Medusan morphospace: phylogenetic constraints, biomechanical solutions, and ecological consequences. *Invertebr. Biol.*, *127*, 265–290.

Franco, E., Pekarek, D. N., Peng, J., & Dabiri, J. O. (2007). Geometry of unsteady fluid transport during fluid structure interactions. *J. Fluid Mech.*, *589*, 125–145.

Haller, G. (2001). Distinguished material surfaces and coherent structures in 3D flid flows. *Physica D*, *149*, 248–277.

Haller, G., & Sapsis, T. (2008). Where do inertial particles go in fluid flows? *Physica D*, *237*, 573–583.

Haller, G., & Sapsis, T. (2009). Localized instability and attraction along invariant manifolds. doi:10.1137/08074324X.

Hansson, L. J., Moeslund, O., Kiorboe, T., & Riisgard, H. U. (2005). Clearance rates of jellyfish and their potential predation impact on zooplankton and fish larvae in a neritic ecosystem (Limfjorden, Denmark). *Mar. Ecol. Prog. Ser.*, *304*, 117–131.

Kawahara, M., Uye, S., Ohtsu, K., & Izumi, H. (2006). Unusual population explosion of the giant jellyfish Nemopilemia nomurai (Scyphozoa: Rhizostomeae) in East Asian waters. *Mar. Ecol. Prog. Ser.*, *307*, 161–173.

Lenz, P. H., & Hartline, D. K. (1999). Reaction times and force production during escape behavior of a calanoid copepod, *Undinula vulgaris*. *Mar. Biol.*, *133*, 249–258.

Madin, L. P. (1988). Feeding behavior of tentaculate predators: in situ observations and a conceptual model. *Bull. Mar. Sci.*, *43*, 413–429.

Matsakis, S., & Conover, R. J. (1991). Abundance and feeding of medusae and their potential impact as predators on other zooplankton in Bedford Basin (Nova Scotia, Canada) during spring. *Can. J. Fish. Aquat. Sci.*, *48*, 1419–1430.

Maxey, M., & Riley, J. (1983). Equation of motion for a small rigid sphere in a nonuniform flow. *Phys. Fluids*, *26*, 883.

Peng, J., & Dabiri, J. O. (2009). Transport of inertial particles by Lagrangian Coherent Structures: application to predator-prey interaction in jellyfish feeding. *J. Fluid Mech.*, *623*, 75–84.

Purcell, J. E. (2005). Predation on zooplankton by large jellyfish, Aurelia labiata, Cyanea capillata and Aequorea aequorea, in Prince William Sound, Alaska. *Mar. Ecol. Prog. Ser.*, *246*, 137–152.

Purcell, J. E., & Decker, M. B. (2003). Effects of climate on relative predation by scyphomedusae and ctenophores on copepods in Chesapeake Bay during 1987–2000. *Limnol. Oceanogr.*, *50*, 376–387.

Purcell, J. E., & Grover, J. J. (1990). Predation and food limitation as causes of mortality in larval herring at a spawning ground in British Columbia. *Mar. Ecol. Prog. Ser.*, *59*, 55–61.

Purcell, J. E., & Mills, C. E. (1991). The correlation between nematocyst types and diets in pelagic Hydrozoa. In D. A. Hessinger & H. M. Lenhoff (Eds.), *The biology of nematocysts* (pp. 463–485). San Diego: Academic Press.

Purcell, J. E., Uye, S., & Lo, W. T. (2007). Anthropogenic causes of jellyfish blooms and their direct consequences for humans: a review. *Mar. Ecol. Prog. Ser.*, *350*, 153–174.

Sapsis, T., & Haller, G. (2009a). Inertial particle dynamics in a hurricane. *J. Atmos. Sci.*, *66*, 2481–2492.

Sapsis, T., & Haller, G. (2009b). Instabilities in the dynamics of neutrally buoyant particles. *Phys. Fluids*, *20*, 017102.

Shadden, S. C., Dabiri, J. O., & Marsden, J. E. (2006). Lagrangian analysis of fluid transport in empirical vortex ring flows. *Phys. Fluids*, *18*, 047105.

Sullivan, B. K., Garcia, J. R., & Klein-MacPhee, G. (1994). Prey selection by the scyphomedusan predator Aurelia aurita. *Mar. Biol.*, *121*, 335–341.

Tang, W., Chan, P. W., & Haller, G. (2010). Accurate extraction of LCS over finite domains, with application to flight safety analysis over Hong Kong International Airport. *Chaos*, *20*, 017502.

Vilela, R. D., de Moura, A. P. S., & Grebogi, C. (2006). Finite-size effects on open chaotic advection. *Phys. Rev. E*, *73*, 026302.

Waggett, R. J., & Buskey, E. J. (2007). Calanoid copepod escape behavior in response to a visual predator. *Mar. Biol.*, *150*, 599–607.